Histidine protonation states are key in the LigI catalytic reaction mechanism

Li Na Zhao,[1,#] Dibyendu Mondal,[2] Weifeng Li,[3] Yuguang Mu,[4] and Philipp Kaldis[1,#]

[1]Department of Clinical Sciences, Lund University, Clinical Research Center (CRC), Box 50332, SE-202 13 Malmö, Sweden

[2]Department of Bioengineering and Therapeutic Sciences, University of California, San Francisco, San Francisco, California

[3]School of Physics, Shandong University, Jinan, 250100, Shandong, China.

[4]School of Biological Sciences, Nanyang Technological University, 60 Nanyang Drive, Singapore, 637551

[#]Correspondence should be addressed to L.N.Z (lina.zhao@med.lu.se) and P.K (Tel: +4673 776 8101; philipp.kaldis@med.lu.se)

Keywords: Histidine protonation state; LigI reaction mechanism; EVB; lactonase

Abstract

Lignin is one of the world's most abundant organic polymers, and 2-pyrone-4,6-dicarboxylate lactonase (LigI) catalyzes the hydrolysis of 2-pyrone-4,6-dicarboxylate (PDC) in the degradation of lignin. The pH has profound effects on enzyme catalysis and therefore we studied this in the context of LigI. We found that changes of the pH mostly affects surface residues, while the residues at the active site are more subject to changes of the surrounding microenvironment. In accordance with this, a high pH facilitates the deprotonation of the substrate. Detailed free energy calculations by the empirical valence bond (EVB) approach revealed that the overall hydrolysis reaction is more likely when the three active site histidines (His31, His33 and His180) are protonated at the ε site, however, protonation at the δ site may be favored during specific steps of reaction. Our studies have uncovered the determinant role of the protonation state of the active site residues His31, His33 and His180 in the hydrolysis of PDC.

Introduction

Lignin, as cross-linked phenolic polymer, is usually integrated into cell walls, and plays a crucial role in conducting water, bacterial resistance, and conferring mechanical strength in plants.[1] It is the second most abundant aromatic compound on earth and its degradation into various metabolites are important steps in the carbon cycle.[2] Lignin has great potential as a renewable source of biofuels or polymer production. However, the production and manufacture in commercially viable ways has proved to be challenging due to difficulties in the oxidative depolymerization of lignin.[3–5]

The enzyme 2-pyrone-4,6-dicarboxylate lactonase (LigI) plays an important role in several lignin degradation pathways, such as the syringate and protocatechuate 4,5-cleavage pathway.[6,7] Notably, among lignin-derived organic compounds, LigI from sphingomonas paucimobilis (S. paucimobilis) catalyzes the hydrolysis of 2-pyrone-4,6-dicarboxylate (PDC) to 4-oxalomesaconate (OMA) and 4-carboxy-2-hydroxymuconate (CHM).[8] PDC as a lignin-derived metabolic intermediate is very stable and the hydrolysis of PDC by LigI is reversible.[9] Sequence analysis and previous studies have concluded that LigI is currently the only identified enzyme in the amidohydrolase superfamily that does not require metals in its active site.[8] Thus the active site and reaction mechanisms of LigI is unique compared to the other members of the amidohydrolase family which require metal ions for their catalytic reaction.[8]

A comprehensive structural and kinetic study of LigI suggested that a single active site residue is required to be deprotonated for the hydrolysis of PDC.[8] Additionally, it was proposed that either Asp248 or His31 is deprotonated for the catalytic activity. The first and only theoretical study of the catalysis by LigI has been done by using a combined quantum mechanics and molecular mechanics (QM/MM) method.[10] In their study, the His31, His33, and His180 were assumed to be singly protonated at the ε site. The pKa of histidine, which is around 6 (in water), readily changes when the surrounding microenvironment changes, especially when it is located at the heart of enzyme active sites, ion channels and metalloproteins.[11] A magic-Angle-Spinning Solid-State NMR spectroscopy study has captured the chemical shift sensitivity towards the tautomeric and protonation state of the structure of LigI.[11] The effect of histidine protonation on the structural dynamic has been studied by molecular dynamics (MD) simulations, which revealed that histidines, as a pH sensor, control the helical structural change of the influenza virus hemagglutinin.[12] Furthermore, histidines protonation is found to be a trigger in the

translocation domain (T domain) of diphtheria toxin.[13]

In our study, we examined the catalytic contributions of different protonation states of His31, His33, and His180 coupled with two different conformations of Asp248. First, we used the semi-microscopic version of the protein dipoles Langevin dipoles (PDLD) model to systematically study how a different pH affects the ionization state of these residues. Second, we evaluate the pKa shift of key residues in coordination with the microenvironment change, such as the mutation, protonation of other ionizable residues, proton transfer, bond forming and breaking as well as protein reorganization. Lastly, we focused on evaluating the reaction energy profile by the empirical valence bond (EVB) in terms of the microenvironment change.

Computational methods

Preparation of the structure of LigI

For the structure preparation, we downloaded all available structures (PDB ID: 4D8L, 4DI8, 4DI9 and 4DIA) of LigI from Protein Data Bank. For the wild type LigI structure preparation, we used the D248A mutant of LigI (PDB ID: 4DI8) as initial structure and then mutated Ala248 back to Asp248. Due to the critical position of the Asp248 and lack of a X-ray structure for wild type bound to substrate, we modeled two Asp248 conformations (I) and (II) as shown in Figure 3b. The Asp248 (I) and (II) conformations have different H-bond patterns: Asp248(II) displays two bonds with His180, which serves to better understand how a small change can influence the simulation as well as the role of His180. The pKa calculations were done by the semi-microscopic of protein dipoles Langevin dipoles (PDLD) model that relax the system at the microscopic level with the linear response approximation (PDLD-LRA).[14] The residues near/at the active site were subjected to the microenvironment changes, and special attention was paid to the following residues: Tyr49, Tyr156, His31, His33, His180, His251, Cys214, Asp179, Asp216, and Arg217.

EVB simulation

The empirical valence bond approach[15–18] was used to simulate the reaction mechanisms as shown in Figure 1. The general polarizable ENZYMIX force field within MOLARIS-XG software were used to represent all atoms.[16] For the substrates at ground (Φ_1^p), intermediate (Φ_2^p) and product state (Φ_3^p), the structures were built by Avogadro,[19] and the charges are

calculated at the HF/6-31G* level by using the Merz-Singh-Kollman (MK) scheme[20] within Gaussian09 software. There are 8 combinations of different protonation states for His31, His33 and His180. Based on the structural analysis, His31 is mainly protonated at the ε position to stabilize the substrate. Here we considered only six combinations (see Table 1). Since we used both Asp248(I) and (II) conformations, a total of 12 systems are generated for the EVB simulations. First, the systems are solvated in a physiological-mimic environment using the surface constrained all-atom protein/solvent (SCAAS) model within MOLARIS-XG. After several rounds of relaxation until the system fully reached the equilibrium state, the final configurations were used for the subsequent EVB studies. The free energy was calculated based on the free energy perturbation/umbrella sampling approach (FEP/US).[18] Note that the long range effects were treated with the local reaction field (LRF) method.[16] 300 *K* was used as the standard temperature for simulation and the calculations of activation free energies.

Results

The sensitivity of ionizable residues towards pH changes

To study pH effects, we evaluate the ionizable residues of LigI at pH 5, 6, 7, 8, and 9. Among the ionizable residues (see Figure 2a) whose protonation state is affected upon the change of the pH, only two residues (Asp179 and His180) are near the active site, the rest (Asp194, Asp261, Asp219, His65, His116, His251, Glu109 and Glu111) are more than 12Å away form the active site (see Figure 2a). Hence, we conclude that at pH 5, the effect of pH on the reaction kinetic is marginal and only limited to a few residues on the surface and substrate. Once the pH increases to the threshold when the two dicarboxylic acids of PDC were deprotonated (mostly at pH 6), the two residues Asp179 and His180 near the active site, start to play an important kinetic role and we will pay special attention during our following EVB study to examine their roles.

Microenvironment changes cause a pKa shift

We estimated the pKa of apo LigI wild-type (pH 8.5) and D248A mutant (pH 8.5), D248A with substrate (pH 8.5), D248A with substrate (pH 6.5) and D248N (pH 4.6) using PDLD-LRA. The pKa of the 11 residues, within 12.5 Å of the reaction center and whose estimated pKa changes above 1, are shown in Figure 2b. Experiments indicated that the kinetic pKa values for the hydrolysis of PDC are around 7.5 and that increasing the pH value from 7.5 to 10, elevates the

conversion of PDC to OMA/CHM.[8] Since His33, Tyr49, Try156, Cys214, and His251 display a pKa shift in the pH range from 7.5 to 10, these residues carry potential for affecting the equilibrium concentrations of the PDC and OMA/CHM during the reaction. Furthermore, the pKa shift between native and D248A at pH 8.5 were calculated and the differences are shown in Figure 2c. His31, Tyr49, Cys214, His33, Asp179 show relatively high sensitivity towards the change in microenvironment. Thus it is important to explore the precise pKa shift due to the local microenvironment changes based on the mutation and electron transfer of nearby residues. In our EVB calculations, we investigated the possible pKa shift by assigning the potential residues different protonation states and by examining how this will affect the kinetic behavior.

Binding and proton affinity of the active site residues

In order to analytically examine the binding affinity of the active site residues towards the substrate, we studied the residues in close proximity of the substrate shown in Figure 3. A hydrogen bond network is formed between Tyr49, Ser77, Arg130, Tyr156, Asn253, Arg183, Arg217, His31 and substrate, which contributes to the stabilization of the substrate. From the K_M value given in 2012 Frank Raushel's paper, we noticed that the mutation of these residues reduce the binding affinity by 4.5x for T49F, 9.7x for R130M, 5x for Y156F, 1.3x for R183M, 1.4x for R217M, and 15x for H31N.[8] Thus, the hydrogen bond network is consistent with the experimental observations. Especially, since the His31-Nε (Hie31) conformation forms a direct hydrogen bond with the O6 of the PDC. Hence, we conclude that His31 is protonated at the ε position and mainly contributes to the stabilization of the substrate. His33 and His180 are two interesting residues, since His180-Nε (Hie180) forms an extra hydrogen bond with the O6 of PDC similar as Hie31 does (see Figure 3). However, in our free energy calculations we found that Hie180 raises the activation barrier by 4 *kcal/mol;* the same as His33-Nε (Hie33).

Water catalyzed reaction profile

The results obtained from the potential energy surface scan of the hydrolysis of the PDC in water shows that (1) the proton transfer from water to Asp-248 accompanies the relocation of the hydroxide ion (OH^-) close to the nucleophilic (around 1.5Å) and the activation energy required for this step is around 20.08 *kcal/mol*; (2) the hydroxide addition accompanies the breaking of the ring and the activation energy required for this step is around 7.53 *kcal/mol*; and

(3) the proton transfer from the hydroxide to the O6 is spontaneous. Meanwhile the hydrogen bond between the proton donor (hydroxide O16) and the proton, lowers the free energy around 2 *kcal/mol* since no hydrogen bond is forming. The simulation in water provides a reference to calibrate the EVB parameters (gas phase shift and coupling constant) and the mechanism for the reaction in enzyme.

The reaction profile catalyzed by LigI

Based on the insight from the reaction profile in water, we know that the proton transfer and the hydroxide attack almost happens in a concerted way. The rate determining step is the proton transfer and the hydroxide oxygen getting close to the electrophile. Here we focus on the rate determining step with the relative free energy profile shown in Figure 5 and Table 1. We found that the lowest reaction barrier for proton transfer (9.95 kcal/mol) is achieved when His31, His33 and His180 are protonated on the ε, δ and δ position, respectively. A single change of the δ or ε ($\delta \leftrightarrow \varepsilon$) protonation state increased the activation barrier around 3 *kcal/mol* for the Φ_1^p to Φ_2^p step.

Figure 6 provides the snapshots of the intermediate state (Φ_2^p) of the six systems we have studied. For the proton transfer step, Hid33 stabilizes the activated hydroxide ion by forming a hydrogen bond, which facilitates the first step of the reaction. However, in the nucleophilic attack, this hydrogen bond makes this step energy unfavorable (Figure 6.1). The combination of Hid31, Hid33 and Hie180 poses a huge activation barrier for the proton transfer to Asp248, which increases the likelihood that the proton transfers to the Hid33 (Figure 6.2). The combination of Hie31, Hid33 and Hie180 moves the hydroxide ion away from the electrophile C1 atom of PDC (Figure 6.3). The combination of Hie31, Hie33 and Hie180 has the best reaction angle for the nucleophilic attack (Figure 6.4). For the combination of Hie31, Hie33 and Hid180, the hydrogen was withdrawn by Asp248 first, and then bridging a hydrogen bond between Asp248 and O6 and O7 of the PDC, which prevents the nucleophilic attack (Figure 6.5). Additionally, the activated hydroxide ion was stabilized by Hie33 and the O12 of PDC, which makes the nucleophilic attack unfavorable. For the combination of Hid31, Hid33 and Hid180, since the important hydrogen bond between Hie31 and PDC O7 is lost, the hydrogen of the hydroxide ion is forming bonds with the O7 and O6 of PDC, which is unfavorable for the nucleophilic attack. Overall, we have observed that protonation of His31 at the ε site provided

stabilization of the substrate. The protonation of His33 at the δ site helps orientate the water molecule and facilitates the proton transfer at first, while the protonation at the ε site contributes a better angle and energy for the nucleophilic attack. Based on the experimental kinetic value (14.04 *kcal/mol*), we assume that the reaction takes the path as indicated in Figure 4 accompanied by the protonation state of His31, His33, and His180 at the ε position.

The reaction profile for the Asp(II) configuration shares the same trend as Asp(I). Hie31, Hid33 and Hid180 provide the lowest activation barrier of 12.07 *kcal/mol* for the proton transfer and the hydroxide ion is getting ready for the subsequent nucleophilic attack, with a single change of $\delta \leftrightarrow \varepsilon$ increasing the activation barrier by 3 to 4 *kcal/mol*. Overall, the difference in the free energy profile between Asp(I) and Asp(II) configurations is within 1.5 *kcal/mol*.

Discussion

Presumably, changes in enzyme's kinetics due to the pH is caused by the variation of the ionizable residues in the enzyme, especially at the active site. In our paper, we combined a systematic study with a realistic model to investigate the change of the enzymatic reaction under different pH conditions. Unexpectedly, the pH change largely affects surface residues of the enzyme and only two residues are near the active site. The most prominent change is observed at the level of substrate, which is deprotonated to the dicarboxylate ion at pH 6. This is further supported by the X-ray crystal structure of the D248N mutant.[8] For the D248N mutant at pH 4.6, there is no substrate or product at the active site. The explanation given in the LigI structural paper[8] is that “the affinity of the active site for substrate or product was reduced under very acidic conditions”. We believe that at acidic conditions, the substrate is protonated and thus becomes too bulky for the active site, or that the substrate may instead interact with the surface residues.

We also found that the pKa values of the active site residues are more subject to changes of the local microenvironment, such as nearby residue mutation, substrate binding, bond forming and breaking, water orientation and protein reorganization, which highlights the need for examination of the protonation sites of histidine residues during the course of the enzyme reaction.

There are implications for *re*-face attack at the carbonyl carbon in Frank Raushel's paper.[8] However, based on the orientation of the Asp248, we believe it is more likely a *si*-face attack. In

our study, we have focused on Asp248 for the withdrawal of the proton. There is a likelihood that His33 withdraws the proton when His31, His33 and His180 are all protonated at the δ sites. Additionally, we were able to define the role of His180. One potential role of His180 is that together with Cys214 and Asp179, it is involved in the proton transfer. We found that when Cys214 was deprotonated, the free energy barrier for the Φ_1^p to Φ_2^p transition can be as low as 8.7 *kcal/mol*. The earliest work on LigI in 1999 indicated that its activity was inhibited by the addition of thiol reagents since cysteine residues are located in a catalytic site.[21] Since a Cys-His-Asp triad has been studied for cysteine proteases, the role of the Cys214 in LigI or the amidohydrolase superfamily, should be studied further in the future.

Overall, we have found that the increase of the pH has considerable effects on residues at the enzyme surface and the decisive change happens on the substrate. Especially the dicarboxylic acid of 2-pyrone-4,6-dicarboxylic acid (PDC) which depronates and converts into dicarboxylate ions at higher pH. LigI has specificity for 2-pyrone-4,6-dicarboxylate but not for 2-pyrone-4,6-dicarboxylic acid.[8] Once the pH increases above a threshold, the pH changes start to affect the residues near the active site. However, we found that the pKa values of the active site residues are more sensitive towards changes of the surrounding microenvironment than to the variation of pH. Therefore, we carefully evaluated the reaction profile by the empirical valence bond (EVB) when the microenvironment changes, namely changes of protonation state of His31, His33 and His180. Our finding is that His31, His33 and His180 are singly protonated at the ε, δ and δ sites, which facilitates the proton transfer. A single change from δ to ε or ε to δ would raise the reaction barrier up to 3 to 4 *kcal/mol*. The His33-Nδ protonated state lowers the free energy barrier at the proton transfer stage by orienting the water molecule and stabilizing the hydroxide ions. The His33-Nε protonated state provides a better angle for the hydroxide ion to approach the electrophile during the nucleophilic attack. We believe that at different pH, His adapts different protonation states (such as δ or ε) since the main component affects the speed of the reaction. The most beneficial pathway in terms of free energy barrier for both proton transfer and nucleophilic attack is that His31, His33 and His180 are all in the ε protonation state. His31 mainly contributes to the binding of the substrate, but there is a likelihood that His31 could withdraw the proton. We have identified that residues His31, His33 and His180 play determinant roles in the catalysis. Furthermore, we have determined that Asp248 acts as a general base to activate water molecules by withdrawing the proton from it. His31 is protonated

on ε site and forms a hydrogen bond with the substrate. The protonation of His33 at δ site facilitates the proton transfer, while the protonation of His33 at ε provides a better angle for nucleophilic attack. We also found that the proton transfer and the movement of the hydroxide ion closer to the electrophile happen in a concerted way.

In summary, this is a detailed study of the different protonation states of three histidine residues at the active site and we uncovered that only certain protonation states confer to the active state of LigI, which is consistent and supported by experimental data.[8] However, the microenvironment exerts more influence than the pH at the active site to fine-tune the chemical equilibrium preferring the forward or reverse reaction. By studying the catalytic residues, we have added more understanding about the underlying mechanisms and helped decipher the biological functions. To the best of our knowledge, this is the first detailed examination of how the histidine protonation states contribute to the catalytic efficiency of LigI.

Since lignin has great potential as the world's largest source of renewable biomass for high-value products such as polymer production, it has been studied in the context of the chemical industry, however, lignin depolymerization is one of the foremost challenges in bioengineering, biorefining and catalysis. Our catalytic study emphasized (i) how the pH influences the substrate; and (ii) that the microenvironment at the active site has profound effects on the catalytic efficiency, which provides theoretical support for future applications in bioengineering.

Acknowledgments

This work is supported by Agency for Science, Technology and Research (A*STAR) International Fellowship (AIF) provided for L.N.Z. P.K is supported by the Faculty of Medicine, Lund University; the Swedish Foundation for Strategic Research Dnr IRC15-0067, and Swedish Research Council, Strategic Research Area EXODIAB, Dnr 2009 1039. L.N.Z. thank Prof. Arieh Warshel for suggestions, discussions, and support, and Dr. Mikolaj Feliks, Dr. Garima Jindal, Dr. Zhen Tao Chu for help in EVB and QM/MM simulation as well as discussions. L.N.Z. thanks Matthew Colopy for his tremendous help and support during the time at USC.

Compliance with ethical standards

Ethical approval is not required for the study.

Data availability

The data that support the findings of this study are available from the corresponding author upon reasonable request.

Conflict of interest

The authors declare that they have no conflict of interest.

References

1. Liu, Q., Luo, L. & Zheng, L. Lignins: Biosynthesis and Biological Functions in Plants. *Int J Mol Sci* **19**, (2018).
2. Kamimura, N. *et al.* Bacterial catabolism of lignin-derived aromatics: New findings in a recent decade: Update on bacterial lignin catabolism. *Environ Microbiol Rep* **9**, 679–705 (2017).
3. Guo, Z.-X., Gandini, A. & Pla, F. Polyesters from lignin. 1. The reaction of kraft lignin with dicarboxylic acid chlorides. *Polymer International* **27**, 17–22 (1992).
4. Schutyser, W. *et al.* Chemicals from lignin: an interplay of lignocellulose fractionation, depolymerisation, and upgrading. *Chem. Soc. Rev.* **47**, 852–908 (2018).
5. Song, Y. *et al.* Gold-catalyzed conversion of lignin to low molecular weight aromatics. *Chem. Sci.* **9**, 8127–8133 (2018).
6. Gold, M. H. & Alic, M. Molecular biology of the lignin-degrading basidiomycete Phanerochaete chrysosporium. *Microbiol Rev* **57**, 605–622 (1993).
7. Kasai, D., Masai, E., Miyauchi, K., Katayama, Y. & Fukuda, M. Characterization of the gallate dioxygenase gene: three distinct ring cleavage dioxygenases are involved in syringate degradation by Sphingomonas paucimobilis SYK-6. *J Bacteriol* **187**, 5067–5074 (2005).
8. Hobbs, M. E. *et al.* Structure and Catalytic Mechanism of LigI: Insight into the Amidohydrolase Enzymes of cog3618 and Lignin Degradation. *Biochemistry* **51**, 3497–3507 (2012).
9. Michinobu, T. *et al.* Molecular Properties of 2-Pyrone-4,6-dicarboxylic Acid (PDC) as a

Stable Metabolic Intermediate of Lignin Isolated by Fractional Precipitation with Na+ Ion. *BCSJ* **80**, 2436–2442 (2007).

10. Zhang, S., Ma, G., Liu, Y. & Ling, B. Theoretical study of the hydrolysis mechanism of 2-pyrone-4,6-dicarboxylate (PDC) catalyzed by LigI. *J Mol Graph Model* **61**, 21–29 (2015).
11. Li, S. & Hong, M. Protonation, Tautomerization, and Rotameric Structure of Histidine: A Comprehensive Study by Magic-Angle-Spinning Solid-State NMR. *J. Am. Chem. Soc.* **133**, 1534–1544 (2011).
12. Kalani, M. R., Moradi, A., Moradi, M. & Tajkhorshid, E. Characterizing a histidine switch controlling pH-dependent conformational changes of the influenza virus hemagglutinin. *Biophys J* **105**, 993–1003 (2013).
13. Perier, A. *et al.* Concerted Protonation of Key Histidines Triggers Membrane Interaction of the Diphtheria Toxin T Domain *. *Journal of Biological Chemistry* **282**, 24239–24245 (2007).
14. Sham, Y. Y., Chu, Z. T. & Warshel, A. Consistent Calculations of pKa's of Ionizable Residues in Proteins: Semi-microscopic and Microscopic Approaches. *J. Phys. Chem. B* **101**, 4458–4472 (1997).
15. King, G. & Warshel, A. A surface constrained all-atom solvent model for effective simulations of polar solutions. *J. Chem. Phys.* **91**, 3647–3661 (1989).
16. Lee, F. S., Chu, Z. T. & Warshel, A. Microscopic and semimicroscopic calculations of electrostatic energies in proteins by the POLARIS and ENZYMIX programs. *Journal of Computational Chemistry* **14**, 161–185 (1993).
17. Warshel, A. & Weiss, R. M. An empirical valence bond approach for comparing reactions in solutions and in enzymes. *J. Am. Chem. Soc.* **102**, 6218–6226 (1980).
18. Kamerlin, S. C. L. & Warshel, A. The EVB as a quantitative tool for formulating simulations and analyzing biological and chemical reactions. *Faraday Discuss.* **145**, 71–106 (2010).
19. Hanwell, M. D. *et al.* Avogadro: an advanced semantic chemical editor, visualization, and analysis platform. *Journal of Cheminformatics* **4**, 17 (2012).

20. Singh, U. C. & Kollman, P. A. An approach to computing electrostatic charges for molecules. *Journal of Computational Chemistry* **5**, 129–145 (1984).
21. Masai, E. *et al.* Genetic and biochemical characterization of a 2-pyrone-4, 6-dicarboxylic acid hydrolase involved in the protocatechuate 4, 5-cleavage pathway of Sphingomonas paucimobilis SYK-6. *J Bacteriol* **181**, 55–62 (1999).

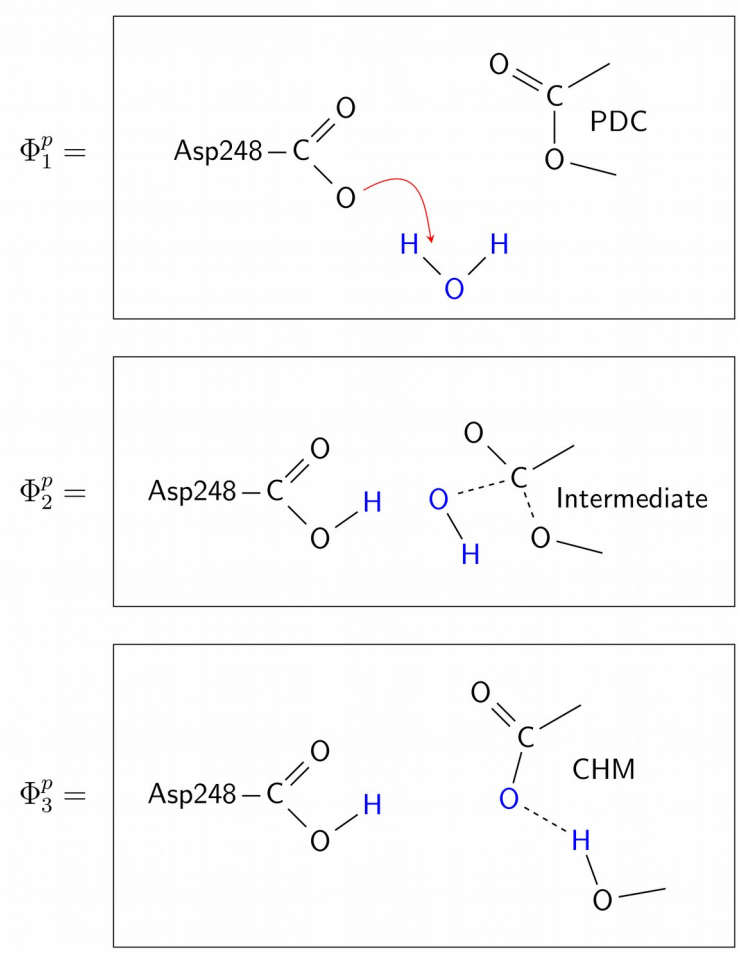

Figure 1: The three EVB resonance states (ϕ_1^p, ϕ_2^p, ϕ_3^p) used to describe the LigI catalytic reaction.

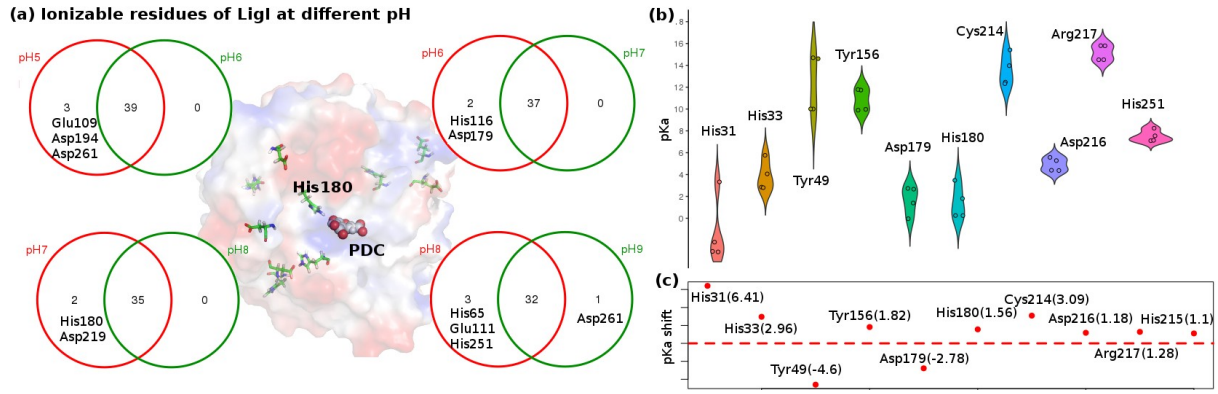

Figure 2: (a) pKa of the ionizable residues of LigI at pH 5 to 9 are compared and shown as Venn diagrams. The number indicates the number of ionized residues. For the unique ones, the residue name as well as residue ID are indicated. These residues, that are affected by the change of the pH, are shown as stick and colored by yellow. The two residues near the active site, Asp179 and His180, are shown as sticks and labeled. (b) Distribution of the pKa values for the 11 residues, within 12.5Å of the reaction center, for native (pH 8.5), D248A mutant (pH 8.5), D248A with substrate (pH 8.5), D248A with substrate (pH 6.5) and D248N (pH 4.6), whose pKa change above 1 between native and D248A mutant, are shown as violin plots. (c) Distribution of the pKa shift during the microenvironment change (WT vs. D248A) at the same pH 8.5 are shown.

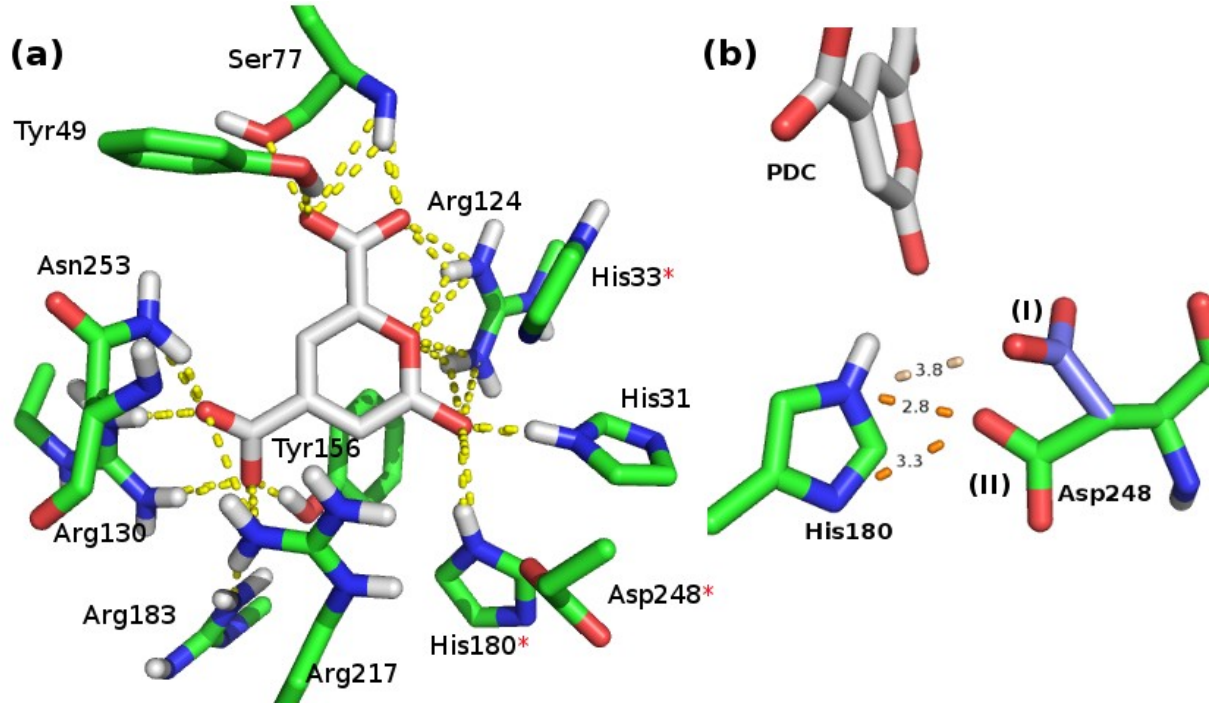

Figure 3: (a) The active site of LigI. The residues within 6Å of PDC are shown as sticks and colored green for C atoms. PDC is shown in stick and colored by element (C: white). The hydrogen bonds are shown with a yellow dashed line. The red star indicates the residues will be discussed further. (b) The two conformations of Asp248 (I) and (II) and their OD1 distance towards His180 are shown. Please note that the proton assignment of histidine is subject to change.

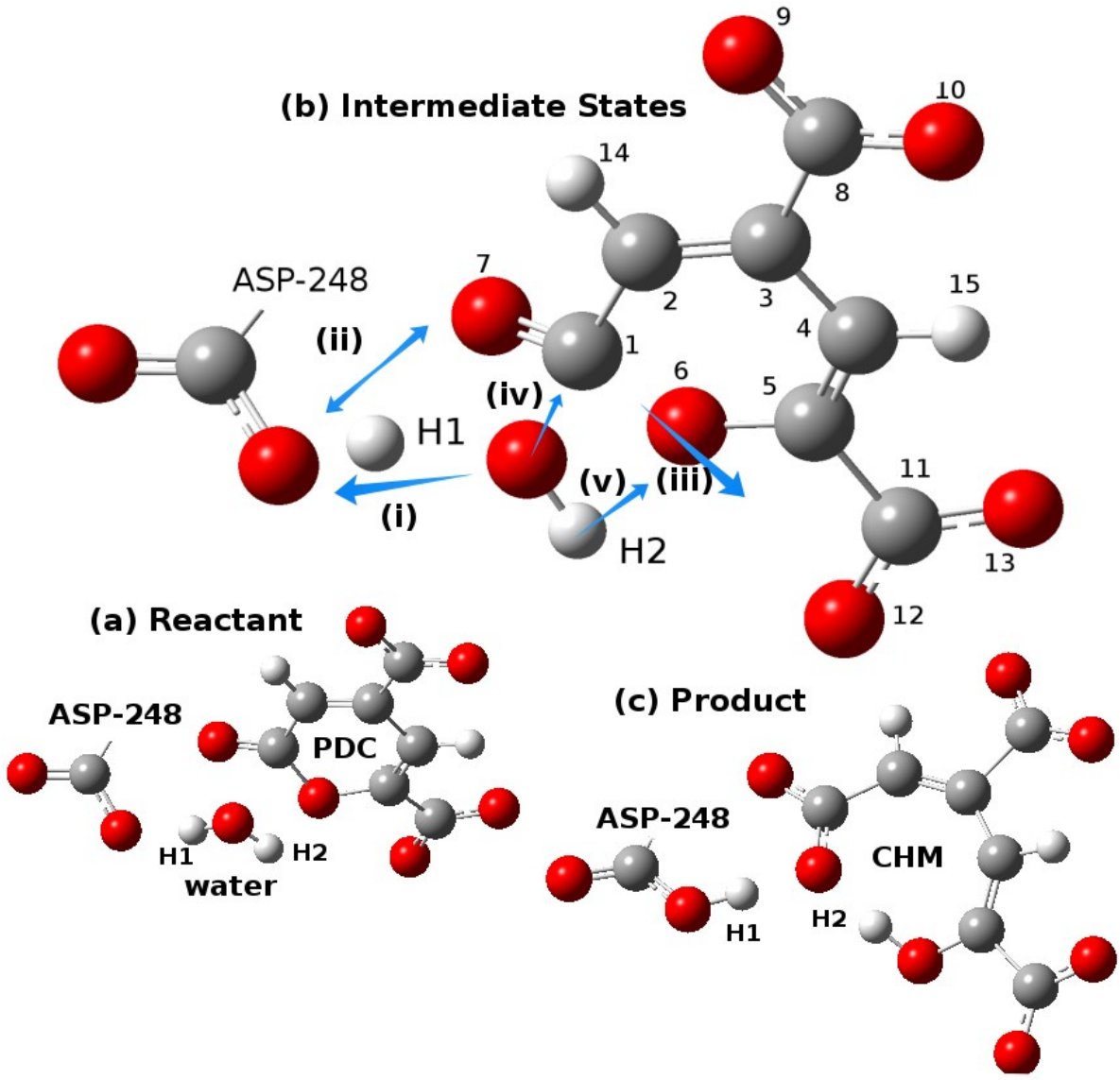

Figure 4: (a) The reactants (PDC, water and Asp248). (b) Intermediate: The blue arrow indicates the movement of the atoms. The five arrows represent different (transition) states [(i) to (v)]. (i) corresponds to the initial step where H1 will be extracted from water and moves to ASP-248; (ii) shows that the H1 may vibrate between oxygen of ASP-248 and the O7 of the ligand; (iii) indicates the ring breaking; (iv) corresponds to the nucleophilic attack step; (v) represents the proton transfer from the O16 to O6 of the ligand. (c) Product (CHM).

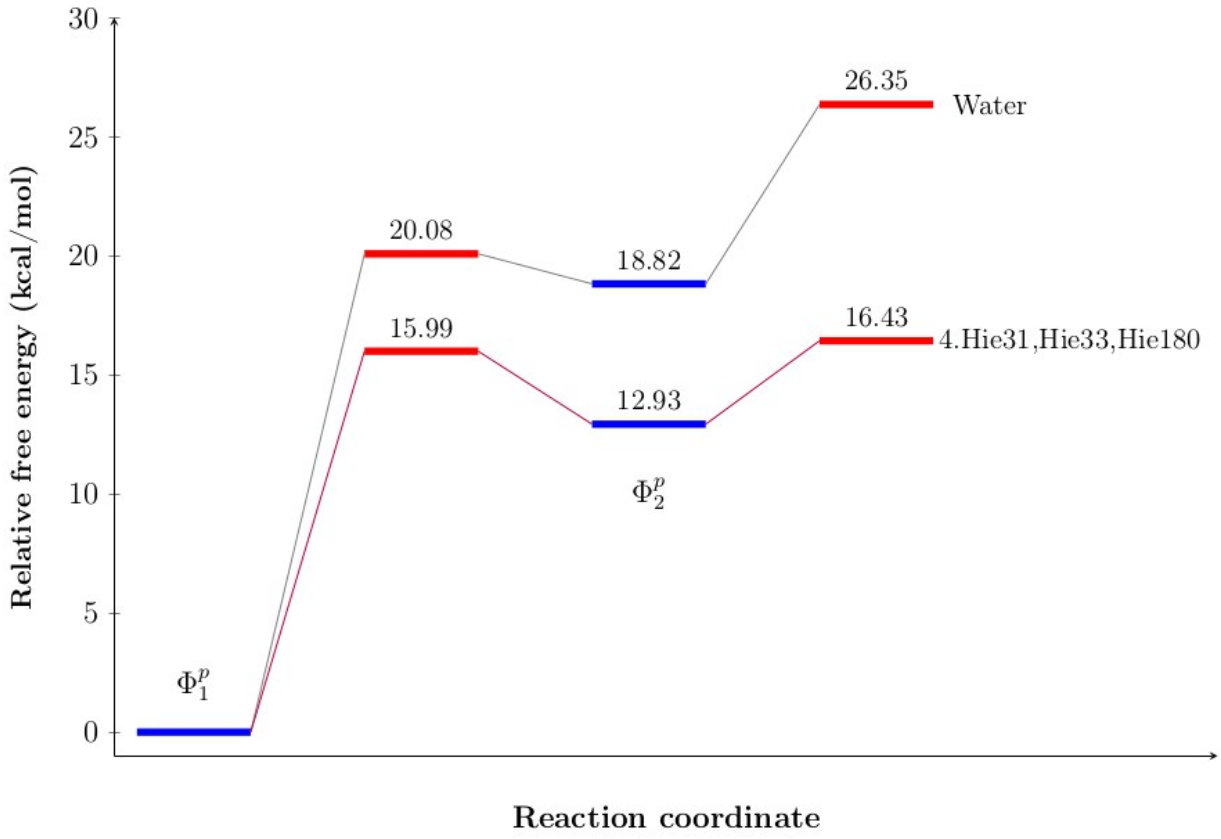

Figure 5: Calculated relative free energy profile in solution and in enzyme for Φ_1^p and Φ_2^p.

systems				calculated free energy			
His protonation state				$\Delta G^{\ddagger}_{PT}$	ΔG	$\Delta G^{\ddagger}_{NA}$	$\Delta G^{\ddagger}$
1	Hie31	Hid33	Hid180	9.95	4.78	48.52	53.3
2	Hid31	Hid33	Hie180	32.4	-	-	-
3	Hie31	Hid33	Hie180	13.97	9.25	31.06	40.31
4	Hie31	Hie33	Hie180	15.99	12.93	3.5	16.43
5	Hie31	Hie33	Hid180	14.27	10.69	11.78	22.47
6	Hid31	Hid33	Hid180	13.07	8.96	51.23	60.19
Ref.				20.08	18.82	7.53	26.35
$\Delta G^{\ddagger}_{Obs} = 15.4 \sim 14.04$ (at pH $6 \sim 8.25$)							

Table 1: The combination of 6 different protonation sites and the calculated free energy. Hie and Hid indicate the protonation is on the ε and δ site, respectively.

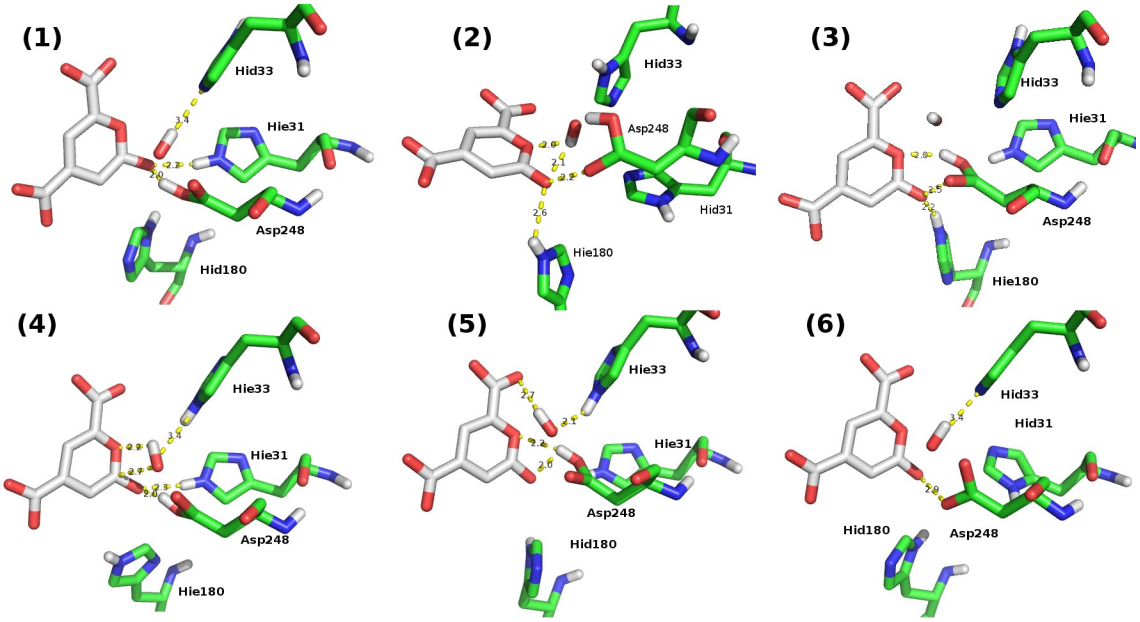

Figure 6: (1)-(6) The intermediate state of $\phi_2{}^p$ of the 6 different systems in the Asp(II) configuration. His31, His33, His180 and Asp248 are shown as stick and colored green for C atoms. PDC is shown as stick and colored white for C atoms. The distance between key atoms are given in Å. Please note that Hie indicates the protonation is on ε site and Hid is on δ site.